

# Separate This, and All of these Things Around It: Music Source Separation via Hyperellipsoidal Queries

Karn N. Watcharasupat and Alexander Lerch

Music Informatics Group, Georgia Institute of Technology, Atlanta, GA, USA

{kwatcharasupat, alexander.lerch}@gatech.edu

## Abstract

Music source separation is an audio-to-audio retrieval task of extracting one or more constituent components, or composites thereof, from a musical audio mixture. Each of these constituent components is often referred to as a “stem” in literature. Historically, music source separation has been dominated by a stem-based paradigm, leading to most state-of-the-art systems being either a collection of single-stem extraction models, or a tightly coupled system with a fixed, difficult-to-modify, set of supported stems. Combined with the limited data availability, advances in music source separation have thus been mostly limited to the “VDBO” set of stems: *vocals*, *drum*, *bass*, and the catch-all *others*. Recent work in music source separation has begun to challenge the fixed-stem paradigm, moving towards models able to extract any musical sound as long as this target type of sound could be specified to the model as an additional query input. We generalize this idea to a *query-by-region* source separation system, specifying the target based on the query regardless of how many sound sources or which sound classes are contained within it. To do so, we propose the use of hyperellipsoidal regions as queries to allow for an intuitive yet easily parametrizable approach to specifying both the target (location) as well as its spread. Evaluation of the proposed system on the MoisesDB dataset demonstrated state-of-the-art performance of the proposed system both in terms of signal-to-noise ratios and retrieval metrics.

## 1 Introduction

Audio source separation is an audio-to-audio retrieval task with the goal of extracting one or more constituent components (“sources”), or composites thereof, from an audio mixture. Music source separation (MSS) is a subtask of audio source separation with a focus on musical audio. In MSS, the terms “sources,” “stems,” or “instruments” are often used interchangeably. In the broadest sense, the term “mixture” in audio source separation refers to the superposition of the sources or their potential transforms (e.g., via room impulse response or digital effects). In source separation literature utilizing deep

learning, however, all of the transformations on the sources are usually assumed to be absorbed into the sources themselves, so that the mixture is a linear instantaneous sum of the ground truth sources.

### 1.1 Fixed-Stem Music Source Separation

Unlike the more widely studied speech source separation task, however, a musical audio mixture often contains a large number of highly correlated wide-band sources overlapping in both time and frequency, and is recorded at a high sampling rate. A common intended downstream usage is of creative nature. This means that (a) the approximate source independence assumption that underlies much of the speech source separation algorithms is almost always violated in real-world musical mixtures, and that (b) the thresholds of acceptable quality for an MSS output are also often considerably higher than those for speech outputs.

These requirements, combined with the historical peculiarities of the data availability [Liutkus *et al.*, 2017; Stöter *et al.*, 2018], have resulted in the MSS field being dominated by a stem-based paradigm with most work focusing on the task of extracting exactly four stems from their mixture: *vocals*, *drum*, *bass*, and the catch-all *others*, collectively known as “VDBO.” A very significant consequence of this stem-based paradigm is that most major milestone systems within MSS have either been (i) a collection of dedicated single-stem extraction models [Uhlich *et al.*, 2017; Takahashi and Mitsufuji, 2017; Takahashi *et al.*, 2018; Stöter *et al.*, 2019; Kim *et al.*, 2021; Takahashi and Mitsufuji, 2021; Luo and Yu, 2023; Lu *et al.*, 2023], or (ii) a tightly coupled model with a fixed set of supported stems [Stoller *et al.*, 2018; Défossez *et al.*, 2019a,b; Hennequin *et al.*, 2020; Défossez, 2021; Kong *et al.*, 2021; Rouard *et al.*, 2023].

While recent systems, both open- and closed-source, have now begun to support some stems beyond VDBO [Hennequin *et al.*, 2020; Rouard *et al.*, 2023], their implementations continue to fall into either of the above categories. Moreover, due to the data-driven nature of practically all modern systems, the exact definition of what a particular “stem” entails is opaque. In practice, the inclusion-exclusion criteria for a particular stem is often a *post hoc* consequence of the training and dataset setups, meaning that even the developers themselves have little *a priori* control over this, and potential end users even less so.

## 1.2 Beyond the Fixed-Stem Paradigm

Several attempts to support MSS beyond a fixed set of stems have been made over the years. Most of these systems rely on some form of query-by-example or conditioning. As early as 2019, although still with VDBO outputs, Meseguer-Brocal and Peeters [2019] used a U-Net with a single decoder to perform MSS, conditioned via multiple feature-wise linear modulation (FiLM) modules [Perez *et al.*, 2017]. This approach and its variations are common with conditional MSS works within and beyond VDBO, as well as in some cross-domain source separation works [Lee *et al.*, 2019; Li *et al.*, 2019; Choi *et al.*, 2021; Jeong *et al.*, 2021; Lin *et al.*, 2021; Gfeller *et al.*, 2021; Slizovskaia *et al.*, 2021; Chen *et al.*, 2022; Liu *et al.*, 2022, 2023; Kong *et al.*, 2023].

Taking the idea of conditional MSS further, some recent works have begun to more substantially challenge the stem-based paradigm. These works are moving beyond a fixed-stem or stem-based paradigm where a single model can extract any source based on some form of additional input that is no longer limited to stem labels. Manilow *et al.* [2022] used gradient ascent to steer a pre-trained MSS model to extract target sources based on auto-tagging predictions. Petermann *et al.* [2023] used a very low-dimensional hyperbolic embedding space to allow similarity-based source separation based on the selected subset of the Poincaré disk. Although this work had a very intuitive interface, the use of very low-dimensional hyperbolic space severely limited the separation fidelity. Wang *et al.* [2022] used a single FiLM conditioning in the U-Net bottleneck to perform few-shot MSS, although its performance was weaker than contemporary models. A similar approach was later taken in Banquet [Watcharasupat and Lerch, 2024], a query-based approach achieving competitive performance to the state-of-the-art fixed-stem HTDemucs [Rouard *et al.*, 2023]. Similar to the system proposed by Wang *et al.* [2022], however, a major limitation of Banquet is that the querying method only specifies a single *point* in the embedding space, around which the relevant signals should be extracted, with no control over the “breadth,” spread, or specificity of the query.

## 1.3 Main Contributions

In this work, we move further beyond the stem-based paradigm, meaning that the extraction target is no longer necessarily treated in a stem-based manner. Instead, we propose to develop a system that can extract any arbitrary target, composite or single-source, as specified by the query. To do so, we generalize query-based MSS beyond *point* query to *region* query, that is, to provide the model with both the “location” and the “spread” of the query. This is loosely similar to the idea of bounding-box queries in image segmentation [Kirillov *et al.*, 2023], but in the abstract embedding space.

We propose using hyperellipsoidal regions as queries, which have a close relationship to the highly generalizable multivariate Gaussian distribution. Specifically, we extend the Banquet model [Watcharasupat and Lerch, 2024] to support a query-by-region operation, resulting in a more customizable source separation method that also supports zero- to few-shots use cases. To the best of our knowledge, our work is the only other system to perform query-based source separation with

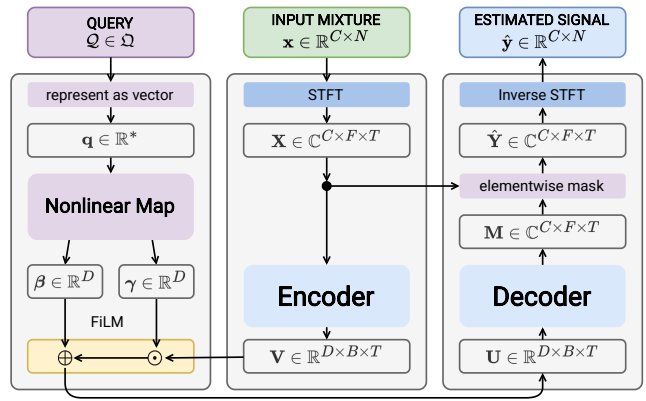


Figure 1: Overview of the Proposed System

region query apart from the aforementioned hyperbolic system [Petermann *et al.*, 2023].

In addition, given the difficulty of evaluating the retrieval performance of query-based MSS systems with a large number of stems and corresponding large timbral diversity, we also introduce a method to evaluate our audio-to-audio MSS system as a retrieval system. This is done by using simple least-squares projection to approximate the presence or absence of a particular source in the model output (i.e., the collection of retrieved items). Given a known target set of sources, we can then determine the extent to which the model has retrieved target sources (i.e., relevant items) or interferences (i.e., irrelevant items) from the mixture (i.e., a collection of all items), despite the system output being that of a superposition of all retrieved signals.

## 2 Proposed System

The overall system in this work is that of a complex-valued time-frequency (TF) masking source separation, with a single query-based embedding adaptation at the bottleneck. The benefit of using a TF-domain masking technique for source separation is that there is a direct connection to the time-domain time-varying convolutive filters, and that the model is incapable of “hallucination” — any information outputted by the model must have already existed in the input. The overall system is visualized in Figure 1.

The general operation of any such system can be described as follows. Let  $\mathbf{x} \in \mathbb{R}^{C \times N}$  be the input audio mixture with  $C$  channels. Let  $\mathbf{X} = \text{STFT}(\mathbf{x}) \in \mathbb{C}^{C \times F \times T}$ , where STFT is the short-time Fourier transform operator,  $F$  is the number of non-redundant frequency bins, and  $T$  is the number of temporal frames. Let  $Q \in \Omega$  be a query representation in some space  $\Omega$ . The overall system can be described by the

sequence of operations:

$$\begin{aligned}
\mathbf{X} &= \text{STFT}(\mathbf{x}) && \in \mathbb{R}^{C \times F \times T} \\
\mathbf{V} &= \text{Enc}(\mathbf{X}) && \in \mathbb{R}^{D \times B \times T} \\
\mathbf{U} &= \text{Cond}(\mathbf{V}, \mathcal{Q}) && \in \mathbb{R}^{D \times B \times T} \\
\mathbf{M} &= \text{Dec}(\mathbf{U}) && \in \mathbb{C}^{C \times F \times T} \\
\hat{\mathbf{Y}} &= \mathbf{M} \circ \mathbf{X} && \in \mathbb{C}^{C \times F \times T} \\
\hat{\mathbf{y}} &= \text{iSTFT}(\hat{\mathbf{Y}}) && \in \mathbb{R}^{C \times N}
\end{aligned} \tag{1}$$

with the mixture encoder  $\text{Enc}: \mathbb{C}^{C \times F \times T} \mapsto \mathbb{R}^{D \times B \times T}$ , the mask decoder  $\text{Dec}: \mathbb{R}^{D \times B \times T} \mapsto \mathbb{C}^{C \times F \times T}$ , and a query conditioning module  $\text{Cond}: (\mathbb{R}^{D \times B \times T}, \mathcal{Q}) \mapsto \mathbb{R}^{D \times B \times T}$ . We will refer to  $\mathbf{V}$  as the mixture embedding,  $\mathbf{U}$  as the conditioning embedding,  $\mathbf{M}$  as the mask, and  $\hat{\mathbf{Y}} \leftrightarrow \hat{\mathbf{y}}$  as the estimated output.

### The Query and the Query Space

The query space  $\mathcal{Q}$  can be defined in different ways. On the one hand,  $\mathcal{Q}$  can simply be a space of one-hot vectors directly representing class labels [Watcharasupat *et al.*, 2024]. On the other hand, it can be extracted from a short audio signal by a pretrained feature extractor such as PaSST [Koutini *et al.*, 2022] to obtain the query embedding [Watcharasupat and Lerch, 2024]. While the former model learned each class directly from the training set, the latter is in principle open to ‘unseen’ queries but entirely dependent on a single short audio example, or the centroid of multiple examples. Neither method allows for the user control of variable levels of “broadness” or specificity.

### FiLM Conditioning

Inspired by other query-based source separation systems [Watcharasupat *et al.*, 2024; Watcharasupat and Lerch, 2024], the conditioning is performed via FiLM at the bottleneck. By representing the query  $\mathcal{Q}$  as a vector, a small fully-connected network (FCN) can be used to map the vector representation to FiLM parameters  $\gamma, \beta \in \mathbb{R}^D$ . These vectors are then used to condition the mixture embedding, yielding

$$\mathbf{U} = \gamma \circ \mathbf{V} + \beta \tag{2}$$

as the resultant embedding for downstream decoding.

### Normalization and Reparametrization

In this work, the mixture encoder and the mask decoder largely follow those of Watcharasupat *et al.* [2023], but with a few additional optimizations to reduce instability during training. Specifically, we introduced (i) global normalization and denormalization similar to that of Demucs [Défossez *et al.*, 2019a; Défossez, 2021], to ensure that the rest of the model is trained independently of the input signal levels, and (ii) reparametrization of the linear layers in the bandsplit and mask estimation modules using the weight normalization [Salimans and Kingma, 2016], which has been shown to improve model convergence [Wu *et al.*, 2020].

## 2.1 Hyperellipsoid as Query

One method to provide the end-user (e.g., musicians) with some level of control over the “broadness” of their query

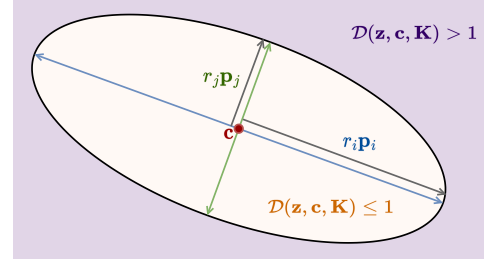


Figure 2: A two-dimensional cross-section of a hyperellipsoid in  $\mathbb{R}^K$ ,  $K \geq 3$ , via a hyperplane  $\{\mathbf{w} \in \mathbb{R}^K : \mathbf{p}_k^T(\mathbf{w} - \mathbf{c}) = 0, \forall k \neq i, j\}$ .

is to allow direct specification of the subset of the abstract space to extract. Petermann *et al.* [2023] have proposed a low-dimensional hyperbolic representation to enable this. However, their method requires the entire system to also follow this low-dimensional modeling, thus limiting the achievable fidelity. Crucially, however, the method proposed by Petermann *et al.* [2023] allows the user to draw an “ellipse,” or a union of multiple “ellipses,” over the Poincaré disk representation of the embedding space.<sup>1</sup>

Inspired by this intuitive control method, we propose the use of a hyperellipsoid in the query embedding space as a query to the model. That is, the model is tasked to obtain all sound components within the mixture whose embeddings lie within the region enclosed by the query hyperellipsoid.

### Query by Region

The concept of source separation using query by region can be formalized as follows. Let  $\mathcal{S} := \{\mathbf{s}_i \in \mathbb{R}^{C \times N}\}$  be the set of sound sources contained within the mixture  $\mathbf{x}$ . As introduced earlier,  $\mathbf{x}$  is the input mixture, which can now be more formally defined as

$$\mathbf{x} := \sum_{\mathbf{s}_i \in \mathcal{S}} \mathbf{s}_i. \tag{3}$$

Let  $\text{Emb}: \mathbb{R}^{C \times N} \mapsto \mathbb{R}^P$  be some embedding operation (e.g. PaSST) on the sound source signals, and let  $\mathcal{Q}$  be some closed region in  $\mathbb{R}^P$ , acting as the query. The target signal  $\mathbf{y}$  of the extraction with input  $\mathbf{x}$  and query  $\mathcal{Q}$  is thus defined as the sum of all the sources whose corresponding embeddings lie within  $\mathcal{Q}$ ,

$$\mathbf{y} = \sum_{\mathbf{s}_i \in \mathcal{Q}} \mathbf{s}_i, \tag{4}$$

where  $\mathcal{Q} := \{\mathbf{s}_i \in \mathcal{S} : \text{Emb}(\mathbf{s}_i) \in \mathcal{Q}\}$ . As mentioned earlier, this work will focus on the case where  $\mathcal{Q}$  is a region enclosed by a hyperellipsoid in the embedding space.

### Region Bounded by a Hyperellipsoid

Generally, the region bounded by a hyperellipsoid in  $\mathbb{R}^P$  can be described by

$$\mathcal{Q}(\mathbf{c}, \mathbf{K}) := \{\mathbf{z} \in \mathbb{R}^P : \mathcal{D}(\mathbf{z}, \mathbf{c}, \mathbf{K}) \leq 1\} \tag{5}$$

<sup>1</sup>Demo: [youtu.be/RKsAMb9z70Y](https://youtu.be/RKsAMb9z70Y). Last accessed: 21 Jan 2025.

where  $\mathbf{c} \in \mathbb{R}^P$  is the center of the hyperellipsoid,  $\mathbf{K} = \mathbf{P}\mathbf{A}\mathbf{P}^\top$  is a positive-definite matrix in  $\mathbb{R}^{P \times P}$ ,  $\mathbf{P}$  is an orthonormal matrix in  $\mathbb{R}^{P \times P}$  defining the principal axes of the hyperellipsoid, and  $\mathbf{r} \in \mathbb{R}_+^P$  is the semi-axis lengths, such that  $\mathbf{A} = \text{diag}(\mathbf{r})^2$ , and

$$\mathcal{D}(\mathbf{z}, \mathbf{c}, \mathbf{K}) = (\mathbf{z} - \mathbf{c})^\top \mathbf{K}^{-1} (\mathbf{z} - \mathbf{c}) \in \mathbb{R}_0^+ \quad (6)$$

is the Mahalanobis distance. In practice,  $\mathbf{K}^{-1}$  above might not be well-conditioned, and is thus replaced by  $\mathbf{K}^\dagger = \mathbf{P}\mathbf{A}^\dagger\mathbf{P}^\top$ , where

$$(\mathbf{A}^\dagger)_{i,i} = r_i^{-2} \text{ if } r_i \geq \epsilon, \text{ else } 0, \quad (7)$$

for some small  $\epsilon$ . A two-dimensional cross-section of a hyperellipsoid in  $\mathbb{R}^K$ ,  $K \geq 3$ , via a hyperplane  $\{\mathbf{w} \in \mathbb{R}^K : \mathbf{p}_k^\top (\mathbf{w} - \mathbf{c}) = 0, \forall k \neq i, j\}$ , is visualized in Figure 2.

The choice to use a hyperellipsoid as the geometric query is due to its close relation to its probabilistic ‘‘counterpart,’’ the multivariate Gaussian distribution, which can approximate many unimodal distributions in high-dimensional space. Additionally, the hyperellipsoidal query lends itself naturally to multimodal extension (i.e., Gaussian mixtures) in a more complex querying scenario beyond the scope of the present work.

### Dimensionality Reduction

Using the PaSST embedding space as the query space is a natural choice as the PaSST space has been shown to be highly discriminative for tasks such as musical instrument classification [Koutini *et al.*, 2022]. The raw 768-dimensional space, however, is not only significantly higher-dimensional than the bottleneck space with  $D = 128$ , but also not empirically full-rank. This leads to unnecessary complexity, memory consumption, and —most importantly— severe numerical stability issues. To alleviate this, we perform principal component analysis (PCA) on the PaSST embedding space to reduce it to a  $D$ -dimensional space. The explained variance of this 128-dimensional reduced space is 91.8% based on the training set. From here, we can assume  $P = D$ .

### Vector Representation of the Query

In this work, the hyperellipsoid  $\mathcal{Q}(\mathbf{c}, \mathbf{K})$  is represented somewhat naively as an  $D(D + 3)/2$ -dimensional vector  $\mathbf{q}$ , by exploiting the symmetry of  $\mathbf{K}$ ,

$$\mathbf{q}^\top = [\mathbf{c}^\top \quad \text{tril}(\mathbf{K})^\top], \quad (8)$$

where `tril` returns lower triangular elements of its input matrix as a vector. The mapping from  $\mathbf{q}$  to the FiLM parameters is done using a small FCN as in MSS Banquet.

## 2.2 Loss Function

### Reconstruction Loss

The reconstruction loss used in this work is the multi-domain multichannel L1SNR loss following Watcharasupat and Lerch [2024].

### Level-Matching Regularization

In order to alleviate the issues with near-silent output raised in Watcharasupat and Lerch [2024], we introduce a simple level-matching regularization  $\mathcal{R}(\hat{\mathbf{y}}; \mathbf{y})$ . Define  $L := \text{dBRMS}(\mathbf{y})$  and  $\hat{L} := \text{dBRMS}(\hat{\mathbf{y}})$ . We have

$$\mathcal{R}(\hat{\mathbf{y}}; \mathbf{y}) = |\hat{L} - L|, \quad (9)$$

with an adaptive weighting

$$\lambda(\hat{\mathbf{y}}; \mathbf{y}) = \lambda_0 + \eta \cdot \Delta\lambda \cdot \text{clamp}_{[0,1]} \left[ \frac{\mathcal{R}(\hat{\mathbf{y}}; \mathbf{y})}{L - L_{\min}} \right], \quad (10)$$

where  $\eta := \mathbb{I}[L > \max(\hat{L}, L_{\min})] \in \{0, 1\}$ ,  $L_{\min}$  is the minimum RMS level in dB,  $\lambda_0$  is the minimum weight,  $\Delta\lambda$  is the weight range, giving  $\lambda_0 + \Delta\lambda$  as the maximum weight. The principle behind the adaptive weighting is to increasingly penalize under-level predictions, while only minimally penalizing over-level predictions.

### Overall Loss

The complete loss function is thus

$$\mathcal{J}(\hat{\mathbf{s}}; \mathbf{s}) = \mathcal{L}(\hat{\mathbf{s}}; \mathbf{s}) + \text{sg}[\lambda(\hat{\mathbf{s}}; \mathbf{s})] \cdot \mathcal{R}(\hat{\mathbf{s}}; \mathbf{s}), \quad (11)$$

where `sg` is the stop-gradient operator. Our repeated preliminary experiments have indicated that the proposed model eventually collapses during training without the level-matching regularization.

## 3 Experimental Setup

### 3.1 Data

This work utilizes MoisesDB [Pereira *et al.*, 2023], a multi-stem music source separation dataset. For comparability, the data splits follow that of Watcharasupat and Lerch [2024]. Abbreviations of the stem names from MoisesDB are shown in Table A.I of the Appendix.

In theory, one desirable approach for training the proposed system would be to expose it to a maximum diversity of queries, in terms of included target sounds, centers, and semi-axis lengths. In practice, however, we continue to be limited by the use of supervised learning, as is the case for nearly all high-fidelity source separation systems to date. This means that the granularity of the included target sounds is dictated by what the dataset provides. This limitation, combined with the sparseness of high-dimensional space, means that naive on-the-fly random sampling of queries is extremely inefficient. The heuristic approach to form a set of valid queries is outlined below.

### Precomputing Valid Queries

For each 10-second sliding-window chunk within a track (‘‘clip’’), we iterate through all possible subsets of available sources. For each subset acting as the set of target sources, we find the smallest enclosing hyperellipsoid that contains all of their embeddings. We eliminate any non-target source with its embedding lying within this hyperellipsoid from the mixture. We then find the largest excluding hyperellipsoid with the same center, such that the embeddings of all the remaining target and non-target sources all lie outside it. Any hyperellipsoid formed by interpolating between the enclosing and the excluding hyperellipsoid would thus specify the same target given the corresponding input mixture. More precise mathematical details are described below.

Let  $\mathcal{U}$  be the set of available sources within each clip, as provided by the dataset. To avoid silent target sources, within each clip, only sources that are at least  $-48$  dBRMS in level

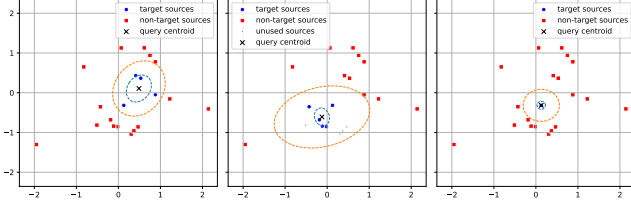


Figure 3: Simplified two-dimensional representation of some possible training queries from the same training data point, meaning that all source embeddings are the same across the three cases. For each case, the valid query with the same input mixture and the target is any ellipse interpolating between the inner (blue) and outer (red) dotted lines. **Left:** The target is a composite of four sources. The input mixture is a composite of all available sources. **Center:** The target is a composite of five sources. Not all available sources are used in the mixture. **Right:** The target is a single source. The input mixture is a composite of all available sources.

were considered to be available. Compute the set of corresponding embeddings  $\mathfrak{Z} := \{\mathbf{z}_j\}$ . For every possible proper subset  $\pi \subset \mathfrak{U}$  corresponding to  $\mathfrak{Z} \subset \mathfrak{Z}$ , we estimate the mean  $\mathbf{c}$  and covariance  $\Sigma = \mathbf{P}_i \Lambda \mathbf{P}_i^T$  of  $\mathfrak{Z}$ , where  $\mathbf{P}$  is orthogonal and  $\Lambda = \text{diag}(\lambda)$ . If  $|\mathfrak{Z}| = 1$ ,  $\mathbf{K}$  is theoretically zero. In practice, we set  $\mathbf{K} = \delta \mathbf{I}$  with a small  $\delta$ . Otherwise,  $\mathbf{K}$  set  $\mathbf{K} := \kappa \Sigma$ , where

$$\kappa := \max_{\mathbf{z} \in \mathfrak{Z}} \mathcal{D}(\mathbf{z}, \mathbf{c}, \Sigma), \quad (12)$$

so that  $\mathbf{z}_j \in \mathcal{E} := \mathcal{Q}(\mathbf{c}, \mathbf{K}), \forall \mathbf{z}_j \in \mathfrak{Z}$ . Define the non-target embedding set as  $\mathfrak{Z}' := \mathfrak{Z} \setminus (\mathfrak{Z} \cup \mathcal{E})$ . Estimate the covariance  $\Sigma'$  of  $\mathfrak{Z}'$  about  $\mathbf{c}$ . Set  $\mathbf{K}' := \kappa' \Sigma'$ , where

$$\kappa' := \min_{\mathbf{z} \in \mathfrak{Z}'} \mathcal{D}(\mathbf{z}, \mathbf{c}, \Sigma'), \quad (13)$$

Assuming that non-zero degenerate eigenvalues of  $\Sigma'$  are extremely rare in practice, we can use the simultaneous orthogonal diagonalization property of positive definite matrices to compute

$$\lambda^\perp := \max\{\text{diag}(\mathbf{P}_i^T \mathbf{K}' \mathbf{P}_i), \lambda\}. \quad (14)$$

Set  $\mathfrak{Z}^\perp := \mathfrak{Z}' \setminus \mathcal{Q}(\mathbf{c}, \mathbf{P}_i \Lambda^\perp \mathbf{P}_i^T)$  to catch any edge cases from numerical issues. Store the centroid  $\mathbf{c}$ , the inclusion radii  $\mathbf{r} := \lambda^{0.5}$ , the exclusion radii  $\mathbf{r}^\perp := (\lambda^\perp)^{0.5}$ , the principal axes  $\mathbf{P}$ , the target source indices  $\pi$ , and the non-target source indices  $\pi^\perp$ .

During training, draw  $\tilde{\mathbf{r}} \sim \text{Unif}(\mathbf{r}, \mathbf{r}^\perp)$ . The query is then defined by  $\mathcal{Q}(\mathbf{c}, \mathbf{P} \text{diag}(\tilde{\mathbf{r}})^2 \mathbf{P}^T)$ . All sources in  $\pi \cup \pi^\perp$  are augmented. The target  $\mathbf{y}$  is formed by linearly summing augmented sources from  $\pi$ , while the input mixture  $\mathbf{x}$  is formed by linearly summing the *same* set of augmented sources from  $\pi \cup \pi^\perp$ .

For the validation set, the radii are formed deterministically with  $\tilde{\mathbf{r}} := (\mathbf{r} + \mathbf{r}^\perp)/2$ . No augmentation was performed to the validation set.

### 3.2 Evaluation Metrics

MSS systems are audio-to-audio retrieval systems. This means that its evaluation has to involve both audio quality evaluation and retrieval quality evaluation. That is, we ask, (1) ‘‘Did the

model output the correct sources’’, and (2) ‘‘Are the model output signals of a high quality?’’. Given that MSS systems output audio *signals*, not logits, confidences, or ranks, these two questions are not easily disentangled in practice.

One approach, that was extremely popular for tackling these evaluations, is that of the BSSEval toolkit [Vincent *et al.*, 2007]. At the time of its development, however, source separation research was largely focused on array source separation of speech signals in a *multichannel linear convolutive* mixture, usually with a maximum of four sources [Vincent *et al.*, 2012]. Unsurprisingly, the de facto standard technique to decompose the error signal into distortion, interference, and artifact signals was designed in that historical context. Despite the enormous usefulness of this decomposition and the resulting metrics, its computation involves orthogonal subspace projections onto the span of the shifted source signals. Amongst other issues [Le Roux *et al.*, 2019; Scheibler, 2022], this projection is numerically unstable and unreliable when there are a large number of highly correlated sources. This limitation has already caused some problems in a four-stem VDBO MSS setup [Stoter *et al.*, 2018], where each output is usually pre-designated to a particular stem. In a query-based system like ours, these problems are amplified, rendering the BSSEval metrics, if numerically computable at all, uninformative for evaluating our system.

However, we still want to answer the two evaluation questions above. To do so, we first rely on the signal-to-noise ratio, a standard audio metric. We then developed a method to approximate the extent to which a source has been retrieved by the model, allowing the system to be evaluated using more convention retrieval metrics.

#### Signal-to-Noise Ratio

In alignment with recent MSS works and the Music Demixing Challenges [Mitsufuji *et al.*, 2022; Fabbro *et al.*, 2024], we evaluate our system using the signal-to-noise ratio (SNR), which is defined by

$$\text{SNR}(\hat{\mathbf{y}}; \mathbf{y}) = 10 \log_{10} \frac{\|\mathbf{y}\|_F^2 + \xi}{\|\hat{\mathbf{y}} - \mathbf{y}\|_F^2 + \xi}, \quad (15)$$

where  $\hat{\mathbf{y}}$  is the test signal and  $\mathbf{y}$  is the reference signal. We use  $\xi = 10^{-6}$  for stability.

SNR is a relatively unforgiving metric in that any sample-level deviation of  $\hat{\mathbf{y}}$  from  $\mathbf{y}$  is treated as an error, regardless of whether this is due to distortions on the (correct) target source, interferences from non-target sources, or just spatial errors. In other words, retrieval errors *will* decrease SNR, but retrieval errors cannot be detected from a decrease in SNR without further inspection. Note also that the consequence of this SNR definition is that a silent  $\hat{\mathbf{y}}$  will produce zero SNR. It is thus important to consider the output levels of the predictions together with the SNR, especially when the SNR is close to zero.

#### Retrieval Metrics

Given the query-based nature of our system, it is important to still evaluate the retrieval performance of the system in a manner that is as independent from the signal quality as possible. Using the same definitions as in Equations (3) and (4), we

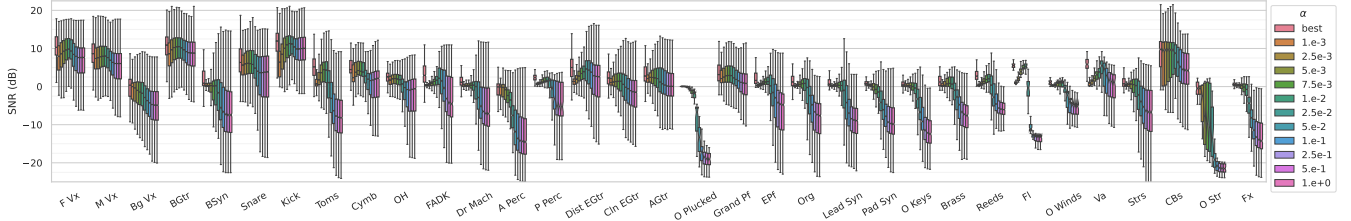


Figure 4: Single-source queries: SNR (dB) distribution by target “stem” over query scale factors,  $\alpha$ , and the clip-wise best factor.

additionally define the set of non-target sources within each clip as  $\mathcal{Y}^\perp := \mathcal{S} \setminus \mathcal{Y}$ . Now, given the corresponding estimated signal  $\hat{\mathbf{y}}$ , we solve for

$$\tilde{\phi} \in \mathbb{R}^{|\mathcal{Y}|}, \tilde{\phi}^\perp \in \mathbb{R}^{|\mathcal{Y}^\perp|} \quad \|\hat{\mathbf{y}} - \tilde{\mathbf{y}}(\tilde{\phi}, \tilde{\phi}^\perp)\|_F^2 \quad (16)$$

where

$$\tilde{\mathbf{y}}(\tilde{\phi}, \tilde{\phi}^\perp) = \sum_{\mathbf{s}_i \in \mathcal{Y}} \tilde{\phi}_i \mathbf{s}_i + \sum_{\mathbf{s}_j^\perp \in \mathcal{Y}^\perp} \tilde{\phi}_j^\perp \mathbf{s}_j^\perp. \quad (17)$$

The weight vectors  $\tilde{\phi} \in \mathbb{R}^{|\mathcal{Y}|}$  and  $\tilde{\phi}^\perp \in \mathbb{R}^{|\mathcal{Y}^\perp|}$  can be obtained using any standard least-squares solver. From here, we normalize elementwise

$$\hat{\phi} := \min\{\mathbf{1}, |\tilde{\phi}|_o\}, \quad \hat{\phi}^\perp := \min\{\mathbf{1}, |\tilde{\phi}^\perp|_o\}. \quad (18)$$

The vectors  $\hat{\phi}$  and  $\hat{\phi}^\perp$  can then be treated as classification “scores” with the corresponding “true” values  $\phi = \mathbf{1}$  and  $\phi^\perp = \mathbf{0}$ . Standard retrieval metrics can now be used to evaluate our system. In this work, we will use accuracy, precision, recall, F1, average precision (AP), mean average precision (mAP), and are under the receiver operating characteristics curve (ROCAUC).

## 4 Results

To evaluate the performance of the system, we chunked each track within the test set into clips using a sliding window of length 10 s and a stride of 1 s. The system was then evaluated using all possible queries, precomputed in the same way as the training and validation sets. For comparability, the model outputs are evaluated in a stem-based manner. It should be emphasized again, however, that the proposed system was never provided the classes of the stems to be extracted during the training or testing.

### 4.1 Single-Source Queries

Given that the inclusion radii,  $\mathbf{r}$ , of a single-source query is theoretically the  $\mathbf{0}^+$  vector, finding the optimal query for the single-source cases can be more challenging than the multi-source cases. For each clip, we query the system using hyper-ellipsoids centered at the centroid of the target embedding and with radii  $\tilde{\mathbf{r}} = \alpha \mathbf{r}^\perp$ , for various  $\alpha \in [10^{-3}, 1]$ . The distribution of the SNR over each target “stem” with various  $\alpha$ ’s are shown in Figure 4. Using the clip-wise best  $\alpha$  and considering only the clips where all sources are included in the mixture, the

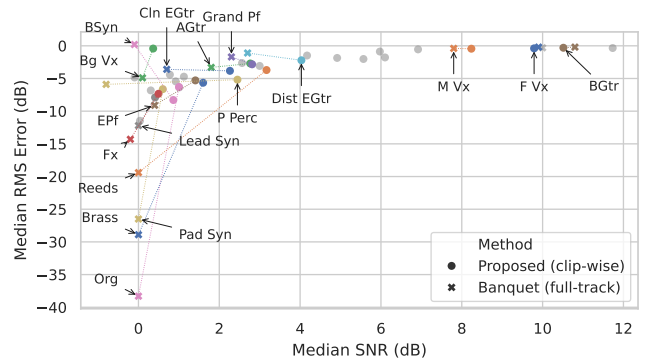


Figure 5: Single-source queries: Plot of the median SNRs (dB) and against median RMS errors (dB) of the proposed method and Banquet (Q:ALL, TE+DA variant). Note again that our method was evaluated clip-wise while Banquet was evaluated over the full track.

median SNRs and root-mean-square (RMS) errors of the proposed method are shown in Figure 5,<sup>2</sup> and compared against the reported results in Banquet (Q:ALL, TE+DA variant) from Watcharasupat and Lerch [2024], where applicable. Note, however, that due to the differences in the evaluation setups, the SNR reported by Watcharasupat and Lerch [2024] was computed over the full track using overlap-add, while ours is computed clip-wise, thus the comparison should only be taken as a rough gauge of relative performance.

Overall, our method performed on par with Banquet on *lead vocals* and *bass guitar*, while performing better on the remainder of the source classes. The most significant improvement over Banquet lies in the performance of sources belonging to “long-tail” instrument classes (*organs*, *synths*, *brass*, *reeds*, *strings*). As noted by Watcharasupat and Lerch [2024], Banquet suffered from collapsed outputs on these sources, as evidenced by the severely negative RMS errors and zero SNRs. While our method still has median RMS errors hovering around  $-6$  dB, this, combined with the positive SNR, indicated that the proposed method can now extract these sources better than Banquet. Interestingly, *flute*, *viola*, and *contrabass* performed better than expected. *Flute* only occurs as a target in 0.4% of the training samples, *contrabass* in 1.0%, and *viola* is not present in the training set at all. Stem classes similar to *viola* and *contrabass* in the training set are also relatively rare, with *cello* at 1.6% and *cello* section at 0.1%.

<sup>2</sup>See Table B.II for the tabular version of Figure 5.

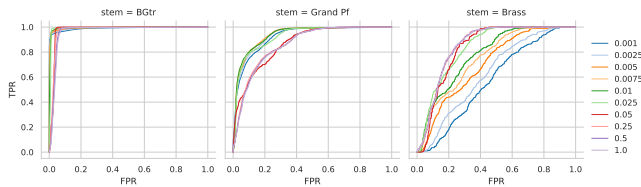


Figure 6: Single-source queries: ROC for lead bass guitar, grand piano, and brass, over different  $\alpha$ .

	AP	Acc.	Precision	Recall	F1
<b>Macro Avg.</b>	0.83	0.76	0.73	0.93	0.81
<b>Micro Avg.</b>	0.86	0.81	0.78	0.93	0.84

Table 1: Summary retrieval metrics for the proposed system in the multi-source query setup.

In terms of  $\alpha$ , we observe that the query width can have significant effects on the model performance. Example effects of  $\alpha$  can be seen in the ROC curves in Figure 6. See Figure B.I for one with every source class. In the example on the left (*bass guitar*), the model is relatively insensitive to  $\alpha$ . For grand piano (middle),  $\alpha \leq 0.025$  (outer cluster of lines) performed similarly amongst one another, but increasing  $\alpha \geq 0.05$  (inner cluster) resulted in a marked drop in ROCAUC. On the other hand, brass (right) performed similarly amongst  $\alpha \geq 0.025$  (outer cluster), but reducing  $\alpha \leq 0.01$  (five inner lines) resulted in a significant drop in the ROCAUCs.

## 4.2 Multi-Source Queries

In the multi-source query cases, both the inclusion and exclusion radii are well-defined. For each clip, we simply query the system using hyperellipsoids centered at the centroid of the target embedding and with radii  $\tilde{r} = (\mathbf{r} + \mathbf{r}^\perp)/2$ . Unlike the single-source case, the inclusion radii for the multi-source case are always strictly non-zero, eliminating the need to iterate through multiple possible queries to obtain a good estimate.

The median SNRs by the number of sources in the mixture and the number of sources in the target are shown in Figure 7. The full distributions are provided in Figure B.III. The corresponding weighted mean average precisions (mAP) by the number of sources in the mixture and the number of sources in the target are shown in Figure 8. The unweighted mAP plot is available in Figure B.II, with a very similar trend as weighted mAP. Summary retrieval metrics are shown in Table 1. The detailed retrieval metrics by source classes are provided in Table B.III.

From Table 1, the overall mAP of the system is 0.83 unweighted and 0.86 weighted. However, the system is clearly more performant in recall than precision. This, in source separation terms, indicates that most of the errors in the output are of an interference nature, rather than a distortion nature.

By computing the ratio of the number of sources in the target to that of the mixture, we can see from Figure 7 that, the larger the number of target sources relative to that of the mixture sources, the better the model performs in terms of SNR. At the same time, for a given number of target sources,

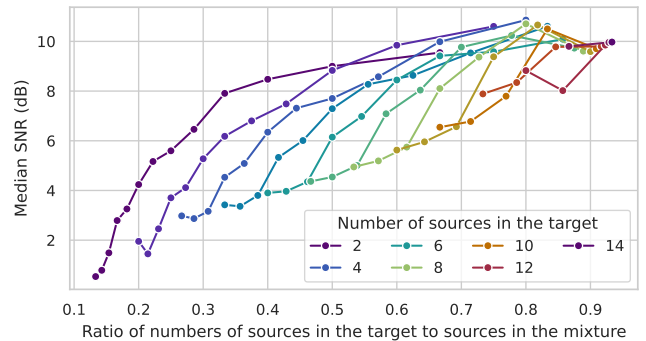


Figure 7: Multi-source queries: Median SNR (dB) by number of sources in the mixture and number of sources in the target.

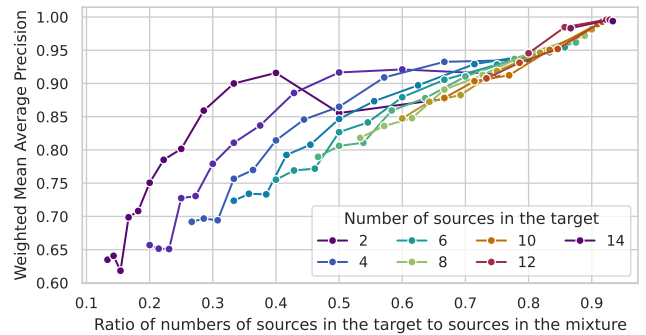


Figure 8: Multi-source queries: Weighted mean average precision by number of sources in the mixture and number of sources in the target.

the larger the number of sources in the mixture, the worse the model performs. This is further supported by Figure 8 which shows a very similar trend in weighted mAP. This trend is somewhat unsurprising from a retrieval perspective, given that the number of relevant items relative to the total size of the collection affects the difficulty of a retrieval task. Given the generally strong performance of the system at a high ratio,

## 5 Conclusion

In this work, we propose a query-based music source separation system using hyperellipsoidal queries. This enables flexible control over both the “timbre” and the “broadness” of the query. The proposed method performs on par or better than state-of-the-art MSS systems, but is — unlike most state-of-the-art systems — not limited to a predefined set of target stems; instead, any source or a set of sources can be extracted as long as their embeddings can collectively be captured using a hyperellipsoid in the query embedding space. In future work, we hope to extend our work to support the use of negative queries, extraction of sources from disjoint regions, and automatic formation of region queries from examples, in order to better support real-world use cases of MSS in creative audio practices.

## References

- Ke Chen, Xingjian Du, Bilei Zhu, Zejun Ma, Taylor Berg-Kirkpatrick, and Shlomo Dubnov. Zero-shot Audio Source Separation through Query-based Learning from Weakly-labeled Data. In *Proceedings of the 36th AAAI Conference on Artificial Intelligence*, Online, February 2022. AAAI.
- Woosung Choi, Minseok Kim, Jaehwa Chung, and Soonyoung Jung. LaSAFT: Latent Source Attentive Frequency Transformation For Conditioned Source Separation. In *Proceedings of the 2021 IEEE International Conference on Acoustics, Speech and Signal Processing (ICASSP)*, pages 171–175. IEEE, June 2021.
- Alexandre Défossez, Nicolas Usunier, Léon Bottou, and Francis Bach. Demucs: Deep Extractor for Music Sources with extra unlabeled data remixed, 2019.
- Alexandre Défossez, Nicolas Usunier, Léon Bottou, and Francis Bach. Music Source Separation in the Waveform Domain, November 2019.
- Alexandre Défossez. Hybrid Spectrogram and Waveform Source Separation. In *Proceedings of the 2021 Music Demixing Workshop at the 22nd International Society for Music Information Retrieval Conference (ISMIR)*, Online, November 2021. ISMIR.
- Giorgio Fabbro, Stefan Uhlich, Chieh-Hsin Lai, Woosung Choi, Marco Martínez-Ramírez, Weihsiang Liao, Igor Gadelha, Geraldo Ramos, Eddie Hsu, Hugo Rodrigues, Fabian-Robert Stöter, Alexandre Défossez, Yi Luo, Jianwei Yu, Dipam Chakraborty, Sharada Mohanty, Roman Solovyev, Alexander Stempkovskiy, Tatiana Habruseva, Nabarun Goswami, Tatsuya Harada, Minseok Kim, Jun Hyung Lee, Yuanliang Dong, Xinran Zhang, Jiafeng Liu, and Yuki Mitsufuji. The Sound Demixing Challenge 2023 – Music Demixing Track. *Transactions of the International Society for Music Information Retrieval*, 7(1):63–84, April 2024.
- Beat Gfeller, Dominik Roblek, and Marco Tagliasacchi. One-Shot Conditional Audio Filtering of Arbitrary Sounds. In *Proceedings of the 2021 IEEE International Conference on Acoustics, Speech and Signal Processing (ICASSP)*, pages 501–505, Toronto, Canada, June 2021. IEEE.
- Romain Hennequin, Anis Khlif, Felix Voituret, and Manuel Mousallam. Spleeter: A fast and efficient music source separation tool with pre-trained models. *Journal of Open Source Software*, 5(50):2154, June 2020.
- Yeong-Seok Jeong, Jinsung Kim, Woosung Choi, Jaehwa Chung, and Soonyoung Jung. LightSAFT: Lightweight Latent Source Aware Frequency Transform for Source Separation. In *Proceedings of the 2021 Music Demixing Workshop at the 22nd International Society for Music Information Retrieval Conference (ISMIR)*, Online, 2021. ISMIR.
- Minseok Kim, Woosung Choi, Jaehwa Chung, Daewon Lee, and Soonyoung Jung. KUIELab-MDX-Net: A Two-Stream Neural Network for Music Demixing. In *Proceedings of the 2021 Music Demixing Workshop at the 22nd International Society for Music Information Retrieval Conference (ISMIR)*, Online, November 2021. ISMIR.
- Alexander Kirillov, Eric Mintun, Nikhila Ravi, Hanzi Mao, Chloe Rolland, Laura Gustafson, Tete Xiao, Spencer Whitehead, Alexander C. Berg, Wan-Yen Lo, Piotr Dollár, and Ross Girshick. Segment Anything, April 2023.
- Qiuqiang Kong, Yin Cao, Haohe Liu, Keunwoo Choi, and Yuxuan Wang. Decoupling Magnitude and Phase Estimation with Deep ResUNet for Music Source Separation. In *Proceedings of the 22nd International Society for Music Information Retrieval Conference (ISMIR)*, pages 342–349, Online, 2021.
- Qiuqiang Kong, Ke Chen, Haohe Liu, Xingjian Du, Taylor Berg-Kirkpatrick, Shlomo Dubnov, and Mark D. Plumbley. Universal Source Separation with Weakly Labelled Data, May 2023.
- Khaled Koutini, Jan Schlüter, Hamid Eghbal-zadeh, and Gerhard Widmer. Efficient Training of Audio Transformers with Patchout. In *Proceedings of the 23rd Annual Conference of the International Speech Communication Association (Interspeech)*, pages 2753–2757, Incheon, Korea, September 2022. ISCA.
- Jonathan Le Roux, Scott Wisdom, Hakan Erdogan, and John R. Hershey. SDR - Half-baked or Well Done? In *Proceedings of the 2019 IEEE International Conference on Acoustics, Speech and Signal Processing (ICASSP)*, pages 626–630, Brighton, United Kingdom, 2019. IEEE.
- Jie Hwan Lee, Hyeong-Seok Choi, and Kyogu Lee. Audio query-based music source separation. In *Proceedings of the 20th International Society for Music Information Retrieval Conference (ISMIR)*, Delft, Netherlands, 2019. ISMIR.
- Bochen Li, Xinzhao Liu, Karthik Dinesh, Zhiyao Duan, and Gaurav Sharma. Creating a Multitrack Classical Music Performance Dataset for Multimodal Music Analysis: Challenges, Insights, and Applications. *IEEE Transactions on Multimedia*, 21(2):522–535, February 2019.
- Liwei Lin, Qiuqiang Kong, Junyan Jiang, and Gus Xia. A Unified Model for Zero-shot Music Source Separation, Transcription and Synthesis. In *Proceedings of the 22nd International Society for Music Information Retrieval Conference (ISMIR)*, pages 381–388, Online, August 2021. ISMIR.
- Xubo Liu, Haohe Liu, Qiuqiang Kong, Xinhao Mei, Jinzheng Zhao, Qiushi Huang, Mark D. Plumbley, and Wenwu Wang. Separate What You Describe: Language-Queried Audio Source Separation. In *Proceedings of the 23rd Annual Conference of the International Speech Communication Association (Interspeech)*, pages 1801–1805, Incheon, Korea, September 2022. ISCA.
- Xubo Liu, Qiuqiang Kong, Yan Zhao, Haohe Liu, Yi Yuan, Yuzhuo Liu, Rui Xia, Yuxuan Wang, Mark D. Plumbley, and Wenwu Wang. Separate Anything You Describe, October 2023.
- Antoine Liutkus, Fabian-Robert Stöter, Zafar Rafii, Daichi Kitamura, Bertrand Rivet, Nobutaka Ito, Nobutaka Ono, and Julie Fontecave. The 2016 Signal Separation Evaluation Campaign. In *Proceedings of the 13th International Conference on Latent Variable Analysis and Signal Separation*, pages 323–332, Grenoble, France, 2017. Springer International Publishing.
- Ilya Loshchilov and Frank Hutter. Decoupled Weight Decay Regularization. In *Proceedings of the 2019 International Conference on Learning Representations (ICLR)*, May 2019.
- Wei-Tsung Lu, Ju-Chiang Wang, Qiuqiang Kong, and Yun-Ning Hung. Music Source Separation with Band-Split RoPE Transformer. In *Proceedings of the 2024 IEEE International Conference on Acoustics, Speech and Signal Processing (ICASSP)*, pages 481–485, Seoul, Korea, Republic of, September 2023. IEEE.
- Yi Luo and Jianwei Yu. Music Source Separation With Band-Split RNN. *IEEE/ACM Transactions on Audio, Speech, and Language Processing*, 31:1893–1901, 2023.
- Ethan Manilov, Patrick O’Reilly, Prem Seetharaman, and Bryan Pardo. Source Separation By Steering Pretrained Music Models. In *Proceedings of the 2022 IEEE International Conference on Acoustics, Speech and Signal Processing (ICASSP)*, pages 126–130, Singapore, Singapore, May 2022. IEEE.
- Gabriel Meseguer-Brocal and Geoffroy Peeters. Conditioned-U-Net: Introducing a Control Mechanism in the U-Net for Multiple Source

- Separations. In *Proceedings of the 20th International Society for Music Information Retrieval Conference (ISMIR)*, pages 159–165, Delft, Netherlands, November 2019. ISMIR.
- Yuki Mitsufuji, Giorgio Fabbro, Stefan Uhlich, Fabian-Robert Stöter, Alexandre Défossez, Minseok Kim, Woosung Choi, Chin-Yun Yu, and Kin-Wai Cheuk. Music Demixing Challenge 2021. *Frontiers in Signal Processing*, 1:808395, January 2022.
- Igor Pereira, Felipe Araújo, Filip Korzeniowski, and Richard Vogl. MoisesDB: A Dataset for Source Separation Beyond 4-Stems. In *Proceedings of the 24th International Society for Music Information Retrieval Conference (ISMIR)*, pages 619–626, Milan, Italy, 2023.
- Ethan Perez, Florian Strub, Harm de Vries, Vincent Dumoulin, and Aaron Courville. FiLM: Visual Reasoning with a General Conditioning Layer. In *Proceedings of the 32nd AAAI Conference on Artificial Intelligence*, New Orleans, LA, USA, December 2017. AAAI.
- Darius Petermann, Gordon Wichern, Aswin Subramanian, and Jonathan Le Roux. Hyperbolic Audio Source Separation. In *Proceedings of the 2023 IEEE International Conference on Acoustics, Speech and Signal Processing (ICASSP)*, Rhodes Island, Greece, June 2023. IEEE.
- Simon Rouard, Francisco Massa, and Alexandre Défossez. Hybrid Transformers for Music Source Separation. In *Proceedings of the 2023 IEEE International Conference on Acoustics, Speech and Signal Processing (ICASSP)*, Rhodes Island, Greece, May 2023. IEEE.
- Tim Salimans and Diederik P. Kingma. Weight normalization: A simple reparameterization to accelerate training of deep neural networks. In *Proceedings of the 30th International Conference on Neural Information Processing Systems, NIPS'16*, pages 901–909, Red Hook, NY, USA, December 2016. Curran Associates Inc.
- Robin Scheibler. SDR - Medium Rare With Fast Computations. In *Proceedings of the 2022 IEEE International Conference on Acoustics, Speech and Signal Processing (ICASSP)*, pages 701–705, Singapore, Singapore, 2022. IEEE.
- Olga Slizovskaia, Gloria Haro, and Emilia Gómez. Conditioned Source Separation for Music Instrument Performances. *IEEE/ACM Transactions on Audio, Speech, and Language Processing*, 29:2083–2095, 2021.
- Daniel Stoller, Sebastian Ewert, and Simon Dixon. Wave-U-Net: A Multi-Scale Neural Network for End-to-End Audio Source Separation. In *Proceedings of the 19th International Society for Music Information Retrieval Conference (ISMIR)*, pages 334–340, Paris, France, 2018. ISMIR.
- Fabian Robert Stöter, Antoine Liutkus, and Nobutaka Ito. The 2018 Signal Separation Evaluation Campaign. In *Proceedings of the 14th International Conference on Latent Variable Analysis and Signal Separation*, pages 293–305, Guildford, United Kingdom, 2018. Springer International Publishing.
- Fabian-Robert Stöter, Stefan Uhlich, Antoine Liutkus, and Yuki Mitsufuji. Open-Unmix - A Reference Implementation for Music Source Separation. *Journal of Open Source Software*, 4(41):1667, September 2019.
- Naoya Takahashi and Yuki Mitsufuji. Multi-Scale multi-band densenets for audio source separation. In *Proceedings of the 2017 IEEE Workshop on Applications of Signal Processing to Audio and Acoustics (WASPAA)*, pages 21–25, New Paltz, NY, October 2017. IEEE.
- Naoya Takahashi and Yuki Mitsufuji. D3Net: Densely connected multidilated DenseNet for music source separation, March 2021.
- Naoya Takahashi, Nabarun Goswami, and Yuki Mitsufuji. MM-DenseLSTM: An Efficient Combination of Convolutional and Recurrent Neural Networks for Audio Source Separation. In *Proceedings of the 16th International Workshop on Acoustic Signal Enhancement*, pages 106–110, Tokyo, Japan, September 2018. IEEE.
- Stefan Uhlich, Marcello Porcu, Franck Giron, Michael Erenkl, Thomas Kemp, Naoya Takahashi, and Yuki Mitsufuji. Improving music source separation based on deep neural networks through data augmentation and network blending. In *Proceedings of the 2017 IEEE International Conference on Acoustics, Speech and Signal Processing (ICASSP)*, pages 261–265, New Orleans, LA, March 2017. IEEE.
- Emmanuel Vincent, Hiroshi Sawada, Pau Bofill, Shoji Makino, and Justinian P. Rosca. First stereo audio source separation evaluation campaign: Data, algorithms and results. In *Proceedings of the 2007 International Conference on Independent Component Analysis and Signal Separation*, pages 552–559, 2007.
- Emmanuel Vincent, Shoko Araki, Fabian Theis, Guido Nolte, Pau Bofill, Hiroshi Sawada, Alexey Ozerov, Vikram Gowreesunker, Dominik Lutter, and Ngoc Q.K. Duong. The Signal Separation Evaluation Campaign (2007-2010): Achievements and Remaining Challenges. *Signal Processing*, 92(8):1928–1936, 2012.
- Yu Wang, Daniel Stoller, Rachel M. Bittner, and Juan Pablo Bello. Few-Shot Musical Source Separation. In *Proceedings of the 2022 IEEE International Conference on Acoustics, Speech and Signal Processing (ICASSP)*, pages 121–125, Singapore, Singapore, May 2022. IEEE.
- Karn N. Watcharasupat and Alexander Lerch. A Stem-Agnostic Single-Decoder System for Music Source Separation Beyond Four Stems. In *Proceedings of the 25th International Society for Music Information Retrieval Conference (ISMIR)*, San Francisco, CA, USA, June 2024. ISMIR.
- Karn N. Watcharasupat, Chih-Wei Wu, Yiwei Ding, Iroro Orife, Aaron J. Hipple, Phillip A. Williams, Scott Kramer, Alexander Lerch, and William Wolcott. A Generalized Bandsplit Neural Network for Cinematic Audio Source separation. *IEEE Open Journal of Signal Processing*, 5:73–81, 2023.
- Karn N. Watcharasupat, Chih-Wei Wu, and Iroro Orife. Facing the Music: Tackling Singing Voice Separation in Cinematic Audio Source Separation. In *Late-Breaking Demo Session of the 25th International Society for Music Information Retrieval Conference*, San Francisco, CA, USA, August 2024. ISMIR.
- Xiaoxia Wu, Edgar Dobriban, Tongzheng Ren, Shanshan Wu, Zhiyuan Li, Suriya Gunasekar, Rachel Ward, and Qiang Liu. Implicit regularization and convergence for weight normalization. In H. Larochelle, M. Ranzato, R. Hadsell, M.F. Balcan, and H. Lin, editors, *Advances in Neural Information Processing Systems*, volume 33, pages 2835–2847. Curran Associates, Inc., 2020.

## SUPPLEMENTARY MATERIALS

### A Additional Details on Data and Experimental Setup

#### A.1 Stem Abbreviation

See Table A.I for the stem abbreviations used in this work.

#### A.2 Training Parametrization

The model presented in this work is trained using an AdamW optimizer [Loshchilov and Hutter, 2019] with an initial learning rate of  $10^{-3}$  and a decay factor of 0.98 per epoch. Each epoch consists of 8192 training batches of 4, using a chunk size of 10 s. Each model is trained for 150 epochs on either an NVIDIA GeForce RTX 3090 or 4090 GPU (both 24 GB).

Abbreviation	Stem
<b>Vx</b>	<b>Vocals</b>
F Vx	Lead Female Singer
M Vx	Lead Male Singer
Bg Vx	Background Vocals
Choir	Human Choir
O Vx	Other Vocals
<b>Bs</b>	<b>Bass</b>
BGtr	Bass Guitar
BSyn	Bass Synthesizer
CBs	Contrabass / Double Bass
Tba	Tuba
Bsn	Bassoon
<b>Dr</b>	<b>Drums</b>
Snare	Snare Drum
Kick	Kick Drum
Toms	Toms
Cymb	Cymbals
OH	Overheads
FADK	Full Acoustic Drumkit
Dr Mach	Drum Machine
<b>Perc</b>	<b>Percussion</b>
A Perc	Atonal Percussion
P Perc	Pitched Percussion
<b>Gtr</b>	<b>Guitar</b>
Dist EGtr	Distorted Electric Guitar
Cln EGtr	Clean Electric Guitar
LS/S Gtr	Lap Steel / Slide Guitar
AGtr	Acoustic Guitar
<b>Plucked</b>	<b>Plucked</b>
O Plucked	Other Plucked
<b>Pf</b>	<b>Piano</b>
Grand Pf	Grand Piano
EPf	Electric Piano
<b>Keys</b>	<b>Keys</b>
Org	Organ / Electric Organ
Lead Syn	Synth Lead
Pad Syn	Synth Pad
O Keys	Other Keys
<b>Winds</b>	<b>Winds</b>
Brass	Brass
Reeds	Reeds
Fl	Flutes
O Winds	Other Wind
<b>Str</b>	<b>Strings</b>
Vn	Violin
Vns	Violin Section
Va	Viola
Vas	Viola Section
Vc	Cello
Vcs	Cello Section
Strs	String Section
O Str	Other Strings
<b>Oth</b>	<b>Others</b>
Fx	Fx
Click	Click Track

Table A.I: Stem Abbreviations

## B Additional Results

### B.1 Single-Source Queries

See Table B.II for the median SNRs (dB) and RMS errors (dB) comparison between the single-source performance of the proposed method and Banquet (Q:ALL, TE+DA variant). Note again that our method was evaluated clip-wise while Banquet was evaluated over the full track.

See Figure B.I for the ROC for each stem over different  $\alpha$ .

"Stem"	SNR (dB)		RMS Error (dB)	
	Ours (clip-wise)	Banquet (full)	Ours (clip-wise)	Banquet (full)
F Vx	9.8	9.9	-0.4	-0.2
M Vx	8.2	7.8	-0.4	-0.4
Bg Vx	0.4	0.1	-0.4	-4.9
BGtr	10.5	10.8	-0.3	-0.2
BSyn	0.9	-0.1	-8.0	0.2
CBs	6.9		-0.6	
Snare	6.0		-0.9	
Kick	11.7		-0.3	
Toms	4.9		-1.8	
Cymb	4.2		-1.5	
OH	2.6		-2.6	
FADK	3.0		-2.6	
Dr	1.1		-3.4	
Mach				
A	-0.1		-4.8	
Perc				
P Perc	2.4	-0.8	-5.1	-5.9
Dist	4.0	2.7	-2.1	-1.1
EGtr				
CIn	2.3	0.7	-3.5	-3.6
EGtr				
AGtr	2.8	1.8	-2.7	-3.3
O Plucked	0.0		-11.5	
Grand	2.8	2.3	-2.8	-1.7
Pf				
EPf	1.4	0.4	-5.2	-9.1
Org	1.0	0.0	-6.2	-38.3
Lead	0.4	0.0	-7.7	-12.2
Syn				
Pad	0.6	0.0	-6.6	-26.5
Syn				
O Keys	0.3		-6.8	
Brass	1.6	0.0	-5.7	-28.9
Reeds	3.2	0.0	-3.7	-19.4
Fl	5.6		-2.0	
O Winds	1.0		-6.4	
Va	6.1		-1.6	
Strs	0.9		-5.4	
O Str	0.8		-4.4	
Fx	0.5	-0.2	-7.3	-14.3

Table B.II: Median SNRs (dB) and RMS errors (dB) comparison between the single-source performance of the proposed method and Banquet (Q:ALL, TE+DA variant). Note again that our method was evaluated clip-wise while Banquet was evaluated over the full track.

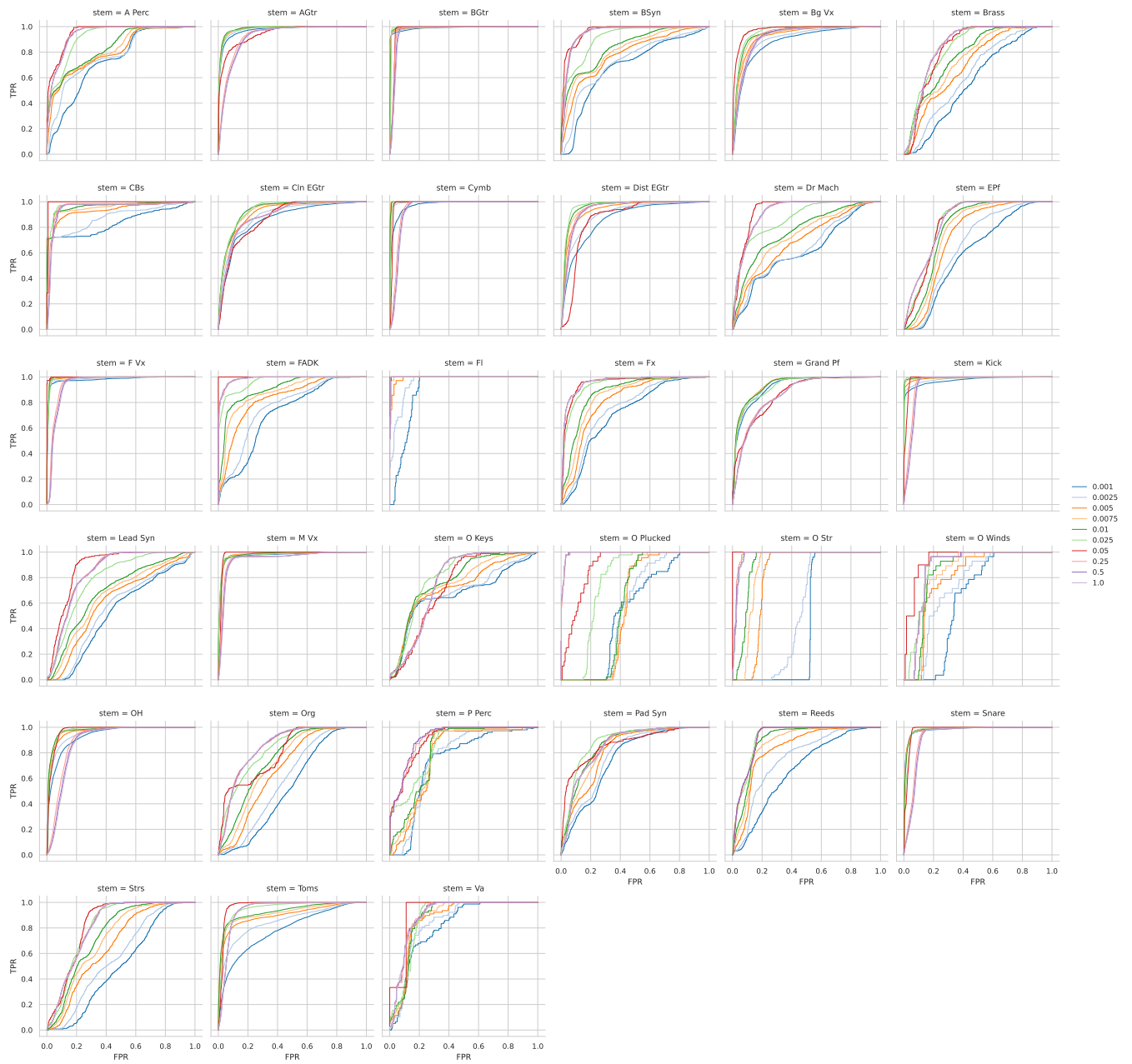


Figure B.I: Single-source query ROC for each source class (“stem”), over different query scale factors  $\alpha$ .

## B.2 Multi-Source Queries

See Figure B.III for the SNR (dB) distribution for multi-source queries by the number of sources in the mixture and the number of sources in the target.

See Figure B.II for the (unweighted) mean average precisions by the number of sources in the mixture and the number of sources in the target.

See Table B.III for the detailed retrieval metrics over source classes.

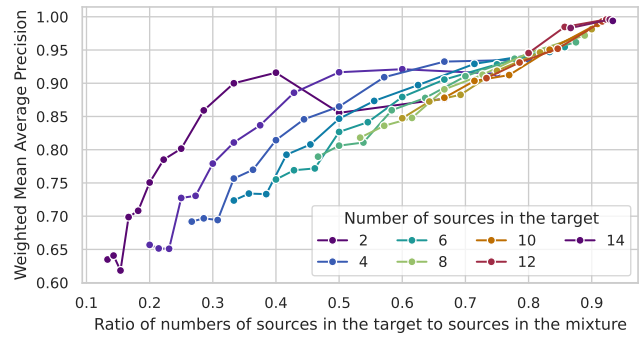


Figure B.II: Weighted mean average precision by number of sources in the mixture and number of sources in the target.

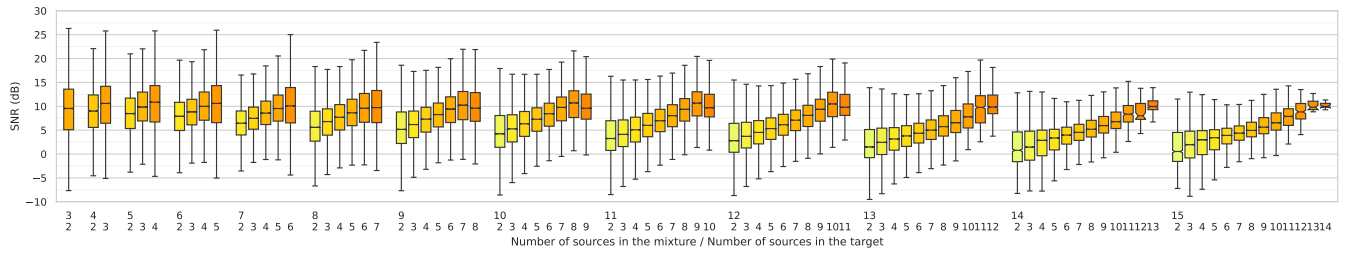


Figure B.III: SNR distribution for multi-source queries by the number of sources in the mixture and the number of sources in the target.

Stem	ROCAUC	PRAUC	AP	Accuracy	Precision	Recall	F1	Threshold
F Vx	0.93	0.92	0.92	0.88	0.85	0.95	0.90	0.22
M Vx	0.97	0.93	0.93	0.91	0.87	0.89	0.88	0.70
Bg Vx	0.90	0.87	0.87	0.82	0.77	0.90	0.83	0.55
BGtr	0.98	0.96	0.96	0.96	0.94	0.98	0.96	0.69
BSyn	0.81	0.84	0.84	0.74	0.69	0.96	0.80	0.18
CBs	0.97	0.97	0.97	0.91	0.89	0.96	0.93	0.43
Snare	0.96	0.94	0.94	0.91	0.88	0.94	0.91	0.61
Kick	0.98	0.97	0.97	0.94	0.93	0.96	0.94	0.58
Toms	0.92	0.91	0.91	0.86	0.83	0.92	0.87	0.58
Cymb	0.96	0.94	0.94	0.94	0.91	0.99	0.95	0.63
OH	0.91	0.87	0.87	0.86	0.82	0.94	0.88	0.51
FADK	0.73	0.69	0.69	0.68	0.62	0.91	0.74	0.17
Dr Mach	0.74	0.69	0.69	0.67	0.61	0.87	0.72	0.48
A Perc	0.84	0.84	0.84	0.75	0.70	0.91	0.79	0.49
P Perc	0.78	0.78	0.78	0.73	0.68	0.97	0.80	0.22
Dist EGtr	0.84	0.84	0.84	0.78	0.74	0.91	0.82	0.49
Cln EGtr	0.75	0.75	0.75	0.66	0.62	0.91	0.73	0.38
AGtr	0.87	0.86	0.86	0.78	0.72	0.85	0.78	0.58
O Plucked	0.67	0.74	0.74	0.62	0.61	0.93	0.74	0.23
Grand Pf	0.84	0.86	0.86	0.71	0.66	0.91	0.76	0.39
EPf	0.75	0.75	0.75	0.67	0.62	0.92	0.74	0.39
Org	0.69	0.72	0.72	0.61	0.59	0.94	0.72	0.27
Lead Syn	0.67	0.69	0.69	0.62	0.59	0.96	0.73	0.26
Pad Syn	0.87	0.88	0.88	0.80	0.79	0.86	0.82	0.61
O Keys	0.69	0.74	0.74	0.65	0.63	0.93	0.75	0.22
Brass	0.66	0.67	0.67	0.60	0.58	0.93	0.71	0.24
Reeds	0.85	0.87	0.87	0.75	0.71	0.93	0.81	0.14
Fl	0.85	0.81	0.81	0.78	0.72	0.93	0.81	0.28
O Winds	0.66	0.75	0.75	0.64	0.63	0.98	0.77	0.12
Va	0.85	0.88	0.88	0.75	0.73	0.88	0.79	0.63
Strs	0.68	0.62	0.62	0.61	0.57	0.95	0.71	0.38
O Str	0.93	0.96	0.96	0.84	0.85	0.91	0.88	0.50
Fx	0.76	0.79	0.79	0.67	0.63	0.90	0.74	0.40
<b>Macro Average</b>	<b>0.83</b>	<b>0.83</b>	<b>0.83</b>	<b>0.76</b>	<b>0.73</b>	<b>0.93</b>	<b>0.81</b>	
<b>Micro Average</b>	<b>0.87</b>	<b>0.86</b>	<b>0.86</b>	<b>0.81</b>	<b>0.78</b>	<b>0.93</b>	<b>0.84</b>	

Table B.III: Retrieval metrics by source classes.